JOURNAL OF THERMOPHYSICS AND HEAT TRANSFER
Vol. 10, No. 2, April–June 1996

# Application of Moving Grid Control Volume Finite Element Method to Ablation Problems

R. E. Hogan,* B. F. Blackwell,† and R. J. Cochran‡
*Sandia National Laboratories, Albuquerque, New Mexico 87185*

**This article presents the solution of two-dimensional axisymmetric ablation problems with unstructured grids. The energy equation is formulated and solved using the control volume finite element method. The exterior shape of the ablating body is determined from a surface energy balance with the interior mesh displaced in response to the surface ablation as if the body was a linear elastic solid. Boundary condition matrices are formulated for both heat of ablation and generalized thermochemical ablation boundary conditions. Computed recession rates are compared to an analytical solution to demonstrate the accuracy and convergence of this approach. Additionally, the practical application of this approach to the ablation of a re-entry vehicle nose tip is presented.**

## Nomenclature

$A$ = area, $m^2$
$B$ = ablation boundary coefficient matrix
$c_h$ = aerodynamic heating transfer coefficient, $kg/(m^2\ s)$
$c_{ij}$ = coefficients in the solid mechanics formulation
$c_p$ = specific heat at constant pressure, J/(kg K)
$e$ = internal energy, J/kg
$i$ = enthalpy, J/kg
$i_c$ = ablator enthalpy at the wall temperature, J/kg
$i_r$ = freestream recovery enthalpy, J/kg
$i_w$ = gas enthalpy at the wall temperature, J/kg
$K$ = global coefficient matrix
$k$ = thermal conductivity, W/(m K)
$M$ = number of nodes along ablating surface
$\dot{m}_c''$ = mass loss rate per unit area, $kg/(m^2\ s)$
$N$ = number of temperature nodes
$n$ = normal coordinate, Eqs. (2) and (3), m
$\hat{\boldsymbol{n}}$ = unit vector normal (inward) to ablating surface
$\dot{Q}$ = heat transfer rate, W
$Q^*$ = heat of ablation, J/kg
$\dot{q}''$ = heat flux, $W/m^2$
$\dot{\boldsymbol{q}}''$ = heat flux vector, $W/m^2$
$r$ = radial coordinate, m
$\boldsymbol{r}$ = right-hand side vector, Eqs. (18) and (19)
$S_i$ = length of exposed boundary for control volume about node $i$, m
$s$ = surface recession or distance along exposed element surface, m
$\dot{s}$ = surface recession rate, m/s
$\dot{\boldsymbol{s}}$ = vector of $M$ unknown surface recession rates, m/s
$T$ = temperature, K
$T_f$ = temperature for fixed temperature ablation, K
$T_{fm}$ = minimum temperature at which ablation begins, K
$T_0$ = initial temperature, K
$\boldsymbol{T}$ = vector of $N$ unknown nodal temperatures, K
$t$ = time, s
$u$ = nodal displacement in the $x$ direction, m
$V$ = volume, $m^3$
$\boldsymbol{Vb}$ = velocity of control volume boundary, m/s
$v$ = nodal displacement in the $y$ direction, m
$x$ = Cartesian coordinate, m
$y$ = Cartesian coordinate, m
$z$ = azimuthal coordinate, m
$\alpha$ = thermal diffusivity or absorptance
$\Delta$ = delta or change
$\varepsilon$ = surface emittance or error
$\xi$ = local coordinate along exposed element surface, m
$\rho$ = density, $kg/m^3$
$\sigma$ = Stefan–Boltzmann constant, $W/(m^2\ K^4)$

*Subscripts*

$c$ = ablator properties at the wall temperature
$i, j, k$ = node indices
$w$ = wall properties
$x$ = component in the $x$ direction
$y$ = component in the $y$ direction
$0$ = initial
$\infty$ = surroundings

*Superscripts*

$e, e+1$ = element indices
$n$ = previous time step
$n+1$ = current time step

## Introduction

ABLATION occurs in many applications, ranging from atmospheric re-entry vehicles to medical procedures using lasers. The ability to predict the ablation rate and the corresponding shape change for problems such as these is important. For example, to successfully design re-entry vehicles, it is necessary to minimize weight, while maintaining thermal protection of the vehicle from the aerodynamic heating of the atmosphere. In the medical community, lasers are presently being used to remove thin layers of dead tissue from burn victims. Numerical models can help to characterize laser parameters so that burned tissue is removed without significant damage to the underlying and surrounding healthy tissue. This article presents a numerical method for predicting the temperature distribution and shape of an ablating, multidimensional body.

Presented as Paper 94-2085 at the AIAA/ASME 6th Joint Thermophysics and Heat Transfer Conference, Colorado Springs, CO, June 20–23, 1994; received Feb. 27, 1995; revision received Nov. 1, 1995; accepted for publication Nov. 3, 1995. 

*Senior Member, Technical Staff, Thermal Sciences Department.
†Distinguished Member, Technical Staff, Thermal Sciences Department. Associate Fellow AIAA.
‡Senior Member, Technical Staff, Thermal Sciences Department. Member AIAA.

Several approaches have been applied to simulate coupled conduction and ablation problems. Some efforts involve allowing the surface nodes to move, while holding the interior nodes fixed, and removing the surface nodes when they come near a neighboring interior node.[1] Other one-dimensional approaches utilize the concept of attaching a grid to the ablating surface.[2] Another one-dimensional approach, known as the Landau transformation,[3] transforms the spatial coordinate over the thickness of the domain so that the transformed coordinate remains between zero and one. Blackwell and Hogan[4] have applied this approach with the control volume finite element method[5] (CVFEM) using exponential differencing for one-dimensional ablation problems. These approaches are generally limited to one-dimensional geometries. For multidimensional problems, more general approaches are required. Blackwell et al.[6] have applied a Landau-type method to move the interior nodes using the concept of spines,[7-10] which constrains interior nodes to remain along predefined lines called spines. The ASCC[11] computer program, an aerospace industry standard for nose-tip design, also utilizes the method of spines. Although computationally efficient, applications of the spine approach have generally been limited to regular or structured grids and are incapable of modeling the complex internal geometry of advanced nose-tip designs.

Our objective is to develop and investigate a method for computing the motion of an unstructured grid in coupled heat conduction and ablation problems. A numerical approach, based on linear elastic solid mechanics,[12] has been developed and applied to example problems of this class. The concept of moving the mesh by assuming the material behaves as a fictitious elastic material was previously proposed by Lynch and O'Neill.[13] The solid mechanics formulation is the critical aspect of this mesh motion approach because it provides the framework for moving an unstructured grid with a small probability of mesh entanglement. As with other finite element solid mechanics simulations, if the elements become extremely distorted, then it may be necessary to remesh the domain and interpolate the temperatures onto the new mesh. Although the analysis presented is for two-dimensional planar/axisymmetric bodies, the procedure is applicable to three-dimensional bodies.

In the work presented in this article, the CVFEM for computing the heat conduction is coupled with both the spines approach and the fictitious solid mechanics approach for computing the grid motion to predict the temperature distribution and boundary shape. Comparisons between predictions and an analytical solution are provided for a one-dimensional problem where the ablation temperature is fixed. Predicted results for a more realistic example, the ablation of a graphite nose tip of a re-entry vehicle, are presented to demonstrate the code capabilities. In this example, the aerodynamic heating is a function of the nose-tip shape and the ablation occurs over a temperature range, not a fixed temperature.

## Governing Equations

### Heat Conduction

The integral form of conservation of energy for a moving and deforming control volume is the starting point for the discussion of this method and is

$$\frac{\mathrm{d}}{\mathrm{d}t}\int\int_V\int \rho e \, \mathrm{d}V + \int\int_A \mathrm{d}\boldsymbol{A}\cdot\dot{\boldsymbol{q}} - \int\int_A \rho i V_b \cdot \mathrm{d}\boldsymbol{A} = 0 \quad (1)$$

The three terms represent the energy storage, heat conduction, and apparent convection of energy due to the grid motion, respectively. This equation is discretized into a system of algebraic equations using the CVFEM. The detailed development of the CVFEM is available in Blackwell and Hogan[4] and Blackwell et al.[6]

### Boundary Conditions

Previously, we presented results for coupled heat conduction and ablation problems for boundary conditions with specified ablation temperature and recession rates.[6] In the work presented here, the ablation boundary conditions are implemented using two different approaches. In the more general approach, referred to as the generalized thermochemical boundary condition, ablation occurs over a temperature range and may be a complex function of temperature and pressure. In the second approach, referred to as the heat of ablation $Q^*$ boundary condition, ablation occurs at a fixed temperature and consumes $Q^*$ energy per unit mass during the ablation process. Example problems demonstrating both approaches for modeling boundary conditions are presented in this article.

#### *General Thermochemical Boundary Conditions*

The boundary condition along the ablating surface is expressed for an aerodynamic heating application in the general form of

$$-k\frac{\partial T}{\partial n} = c_h(i_r - i_w) + \alpha_w \dot{q}_r'' - \varepsilon_w\sigma(T_w^4 - T_\infty^4) - \dot{m}_c''(i_w - i_c) \quad (2)$$

where $c_h$ is an aerodynamic heating heat transfer coefficient based on enthalpy ($i$) difference driving potential $\dot{q}_r''$ is an input radiation heat flux, and $\dot{m}_c''$ is the mass flux that may be a complex function of surface temperature and pressure. In this work, the mass flux is represented as a tabular function of temperature and pressure. Both the mass flux and the wall temperature are unknowns in Eq. (2). The iteration variable for this formulation is the wall temperature. This boundary condition formulation will be referred to in this article as the generalized thermochemical boundary condition.

#### *$Q^*$ Boundary Conditions*

In addition to Eq. (2), we have applied a simplified heat of ablation model that replaces the enthalpy difference at the wall with a heat of ablation term and constrains ablation to take place at a fixed surface temperature. The heat of ablation boundary condition is

$$-k\frac{\partial T}{\partial n} = c_h(i_r - i_w) + \alpha_w \dot{q}_r'' - \varepsilon_w\sigma(T_w^4 - T_\infty^4) - \dot{m}_c'' Q^* \quad (3)$$

where $Q^*$ is the heat of ablation (energy per unit mass consumed in the ablation process) and is assumed constant for a given material. In this formulation, the wall temperature is known and the mass flux (recession rate) is computed from the energy balances for surface nodes. This boundary condition formulation will be referred to as the $Q^*$ boundary condition.

### Mesh Motion Procedure

During the ablation process, material is lost from the surface. The rate of material loss is determined by an energy balance along the ablating surface. In the formulation presented here, the surface nodes are attached to the ablating surface and are permitted to move with it. The mesh motion is modeled by assuming that the mesh behaves as a linear elastic solid. This approach, previously considered by Lynch and O'Neill,[13] has not been widely applied. Using this approach readily allows the use of an unstructured mesh and provides a logical extension to three-dimensional problems. The displacement of nodes along the ablating surface is determined by a surface energy balance. For the two-dimensional axisymmetric problems presented here, we have applied a two-dimensional linear elastic solid mechanics model to predict the motion of the interior nodes.

For simplicity, a planar formulation for the solid mechanics was used. Because the solid mechanics approach is being used

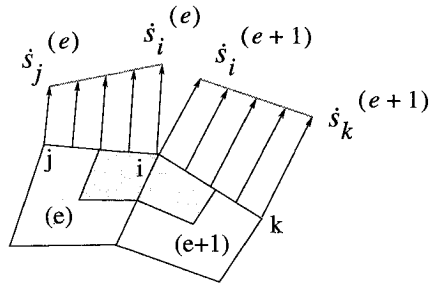


**Fig. 1 Specification of linear variation in recession rate along ablating boundaries of individual elements. Variations of enthalpy difference are similarly interpolated.**

only to move the mesh, with no interest in the accuracy of computed stresses or strains, the coupling of the planar solid mechanics formulation and the axisymmetric thermal formulation is acceptable.

The equations governing the mesh motion can be expressed in terms of the nodal displacements as

$$\frac{\partial}{\partial x}\left(c_{11}\frac{\partial u}{\partial x} + c_{12}\frac{\partial v}{\partial y}\right) + c_{33}\frac{\partial}{\partial y}\left(\frac{\partial u}{\partial y} + \frac{\partial v}{\partial x}\right) = 0 \quad (4)$$

$$c_{33}\frac{\partial}{\partial x}\left(\frac{\partial u}{\partial y} + \frac{\partial v}{\partial x}\right) + \frac{\partial}{\partial y}\left(c_{12}\frac{\partial u}{\partial x} + c_{22}\frac{\partial v}{\partial y}\right) = 0 \quad (5)$$

where the $c_{ij}$ coefficients are functions of the properties of the fictitious material, in particular, functions of the modulus of elasticity and Poisson's ratio. The actual values of the $c_{ij}$ coefficients depend on the solid mechanics assumptions, either plane strain or plane stress in two dimensions.[12] In the work presented here, the plane strain formulation is used and structural properties are representative of steel. The structural properties are used exclusively for moving the mesh and have no direct impact on the thermal aspects of the problem (other than how the mesh moves).

During the ablation process, the temperature and shape of the body are determined by a surface energy balance. Along the ablating surface, the motion of the mesh is coupled to the thermal boundary conditions through the recession rate $\dot{s}$. In our approach, the surface nodes are assumed to be attached to the receding surface and their movement is specified using a local surface normal and recession rate. Over a time step of $\Delta t$, the displacement boundary conditions for each ablating node are computed from

$$\begin{bmatrix} u \\ v \end{bmatrix} = \begin{bmatrix} \dot{s}\Delta t n_x \\ \dot{s}\Delta t n_y \end{bmatrix} \quad (6)$$

where $n_x$ and $n_y$ are the $(x, y)$ components of $\hat{\boldsymbol{n}}$, the normal unit vector into the surface at this node.

### Boundary Condition Element Matrices

Element matrices will be developed in this section for the ablating boundary conditions. Figure 1 shows the variation of recession rate along the ablating boundary and will be used to develop the boundary condition element matrices for the contribution of element $e$ to the control volume for node $i$. In this development, the recession rates are assumed to be nodal variables, $\dot{s}_i^{(e)} = \dot{s}_i^{(e+1)}$.

#### *General Thermochemical Boundary Conditions*

For implementing the generalized thermochemical ablation boundary conditions, the heat flux associated with ablation is the product of the mass flux and the enthalpy difference driving potential, and is given by

$$\dot{q}^{(e)} = \dot{m}_c''(i_w - i_c) \quad (7)$$

In this formulation, the mass flux and the enthalpy may be complex, but known functions of temperature and pressure. For example, thermochemical ablation[2] of graphite will be assumed in one of the example problems presented. To develop the ablation boundary condition matrix, consider the contribution of element $e$ to the energy balance on node $i$, which is given by

$$\dot{Q}_i^{(e)} = \int_{S_i^{(e)}} \dot{m}_c''(i_w - i_c)2\pi r \, ds \quad (8)$$

In this development, the mass flux will be expressed as the product of $\rho$ and $\dot{s}$ of the ablating surface as

$$\dot{m}_c'' = \rho^{(e)}\dot{s} \quad (9)$$

It will be assumed that both the recession rate and the enthalpy difference vary linearly along the exposed surface of the element. For the recession rate, this variation is written in terms of the recession rate at the nodes as

$$\begin{aligned} \dot{s} &= \tfrac{1}{2}(1 + \xi)\dot{s}_i + \tfrac{1}{2}(1 - \xi)\dot{s}_j \\ &= \tfrac{1}{2}(\dot{s}_i + \dot{s}_j) + \tfrac{1}{2}(\dot{s}_j - \dot{s}_i)\xi \end{aligned} \quad (10)$$

The enthalpy difference between the gas and the ablator (both at the wall temperature) is also assumed to vary linearly with position along the ablating surface as

$$\begin{aligned} \Delta i &= \tfrac{1}{2}(1 + \xi)\Delta i_i + \tfrac{1}{2}(1 - \xi)\Delta i_j \\ &= \tfrac{1}{2}(\Delta i_i + \Delta i_j) + \tfrac{1}{2}(\Delta i_j - \Delta i_i)\xi \end{aligned} \quad (11)$$

where $\Delta i = (i_w - i_c)$. After performing the integration indicated by Eq. (8), the contribution of this element ablation boundary condition matrix for node $i$ at time $n + 1$ can be written as

$$\dot{Q}_i\big|_{\text{abl}}^{(e)} = 2\pi\frac{S_{ij}^{(e)}}{2}\rho^{(e)}\frac{(r_i + r_j)}{2}\frac{1}{4}[\Delta i_i \; \Delta_j]^{(e)} \times \left\{\begin{bmatrix} \frac{7}{3} & \frac{2}{3} \\ \frac{2}{3} & \frac{1}{3} \end{bmatrix} - \frac{(r_j - r_i)}{(r_j + r_i)}\begin{bmatrix} \frac{17}{12} & \frac{3}{12} \\ \frac{3}{12} & \frac{1}{12} \end{bmatrix}\right\}\begin{bmatrix} \dot{s}_i^{n+1} \\ \dot{s}_j^{n+1} \end{bmatrix}^{(e)} \quad (12)$$

where the first matrix in brackets represents the planar contributions and the second matrix the axisymmetric contributions. For the control volume about node $j$, the contribution of this element is

$$\dot{Q}_j\big|_{\text{abl}}^{(e)} = 2\pi\frac{S_{ij}^{(e)}}{2}\rho^{(e)}\frac{(r_i + r_j)}{2}\frac{1}{4}[\Delta i_i \; \Delta i_j]^{(e)} \times \left\{\begin{bmatrix} \frac{1}{3} & \frac{2}{3} \\ \frac{2}{3} & \frac{7}{3} \end{bmatrix} + \frac{(r_j - r_i)}{(r_j + r_i)}\begin{bmatrix} \frac{1}{12} & \frac{3}{12} \\ \frac{3}{12} & \frac{17}{12} \end{bmatrix}\right\}\begin{bmatrix} \dot{s}_i^{n+1} \\ \dot{s}_j^{n+1} \end{bmatrix}^{(e)} \quad (13)$$

The contributions of each element along the ablating surface are added into the global right-hand side (RHS) to complete the conservation of energy statement. Assembly of these boundary condition contributions is done on an element-by-element basis.

#### *Q* Boundary Conditions*

For $Q^*$ ablation boundary conditions, the magnitude of the heat flux associated with ablation is assumed to be the product

of the material density, the recession rate, and the heat of ablation, and is given by

$$\dot{q}^{(e)} = \rho^{(e)} \dot{s} Q^* \tag{14}$$

where $\rho^{(e)}$ is the element material density. Hence, the element $e$ contribution to the energy balance on the control volume for node $i$ is given by

$$\dot{Q}_i^{(e)} = \rho^{(e)} Q^* \int_{S_i^{(e)}} \dot{s} 2\pi r \, ds \tag{15}$$

Again, the recession rate is assumed to vary linearly with position along the exposed surface [see Eq. (10)]. After performing the integration indicated by Eq. (15), the element ablation boundary condition matrix at time $n + 1$ can be written as

$$\begin{bmatrix} \dot{Q}_i \\ \dot{Q}_j \end{bmatrix}_{\text{abl}}^{(e)} = 2\pi \frac{S_{ij}^{(e)}}{2} \rho^{(e)} Q^* \frac{(r_i + r_j)}{2} \left\{ \begin{bmatrix} \frac{3}{4} & \frac{1}{4} \\ \frac{1}{4} & \frac{3}{4} \end{bmatrix} + \frac{(r_j - r_i)}{(r_j + r_i)} \begin{bmatrix} -\frac{5}{6} & -\frac{1}{6} \\ \frac{1}{6} & \frac{5}{6} \end{bmatrix} \right\} \begin{bmatrix} \dot{s}_i^{n+1} \\ \dot{s}_j^{n+1} \end{bmatrix}^{(e)} \tag{16}$$

where the $n + 1$ superscript denotes the current time step. Expressed in terms of the product of a coefficient matrix and the recession rate vector, the ablation boundary terms given by Eq. (16) can be written as

$$\begin{bmatrix} \dot{Q}_i \\ \dot{Q}_j \end{bmatrix}_{\text{abl}}^{(e)} = [B]^{(e)} \begin{bmatrix} \dot{s}_i^{n+1} \\ \dot{s}_j^{n+1} \end{bmatrix}^{(e)} \tag{17}$$

where $[B]^{(e)}$ is the ablation boundary coefficient matrix for the element.

If the recession rates in Eq. (17) were explicitly known, then these terms would be directly added into the right-hand vector of the global system of equations. Because the recession rate and the coefficient matrix for the temperature vector are coupled through the mesh motion, these nodal recession rates will be kept as explicit unknowns in the global system of equations. Contributions similar to Eq. (17) will only exist for those elements along the ablating surface. This formulation and details of the solution procedure are discussed in detail next.

### Global System of Equations

*General Thermochemical Boundary Conditions*

The discrete global system of equations describing heat conduction with generalized thermochemical ablation boundary conditions can be expressed in matrix form as

$$[K(T, \dot{s})]\, T^{n+1} = r(T, \dot{s}) \tag{18}$$

where $K$ is the $(N \times N)$ global coefficient matrix containing contributions from the capacitance, conduction, volume change, and boundary condition terms and $T^{n+1}$ is the vector of $N$ unknown nodal temperatures at time $n + 1$. In this formulation, the global coefficient matrix depends on both temperature and the recession rate. The RHS also depends on the recession rate, which is a complex function of temperature and pressure. There are $N$ unknown nodal temperatures and $M$ unknown nodal recession rates, but only $N$ discrete conservation of energy equations represented by Eq. (18). The additional $M$ relationships between temperature and recession rate are available in the form of the mass loss tabular function for the ablating material. Consequently, an iterative procedure is used to obtain a set of temperatures and recession rates satisfying conservation of energy for each time step.

To advance the solution a time step, begin with $T^n$ and $\dot{s}^n$ from the previous time step as initial guesses and iterate using an iteration index, i. Set $\dot{s}^i = \dot{s}^n$ and $T^i = T^n$.

1. Move the mesh based on $\dot{s}^i$
2. For ablating nodes, (temperature above minimum for ablation), apply the ablation boundary conditions by computing the mass flux and enthalpy difference driving potential and adding ablation contributions to right-hand-side vector (Eq. (18))
3. Compute a new vector of temperatures, $T^{i+1}$, from global system of equations (Eq. (18))
4. Evaluate a new $\dot{s}^{i+1} = \dot{s}(T, P)$
5. Compute an average change of temperature for ablating nodes between the $i+1$ and $i$ iteration using $\varepsilon = \frac{1}{M} \sum_{j=1}^{M} \left| T_j^{i+1} - T_j^i \right|$,
6. If $\varepsilon \geq \varepsilon_{max}$, then, using $\dot{s}^{i+1}$, return to Step 1

**Fig. 2 Flow chart showing the iterative procedure for solving conservation of energy with generalized thermochemical ablation boundary conditions.**

Figure 2 shows a flow chart describing the iteration procedure for computing the unknown temperatures and recession rates to advance the solution over a time step with the generalized thermochemical form of the ablation boundary conditions. It is assumed at the beginning of this iterative process that initial guesses of the temperature and recession rate are available from the previous solution. For the first time step, the recession rates are assumed to be zero.

*Q* Boundary Conditions*

For the $Q^*$ ablation boundary condition formulation, the global system of equations is given by

$$[K(T, \dot{s})]\, T^{n+1} + [B(T)]\, \dot{s}^{n+1} = r(T, \dot{s}) \tag{19}$$

where $B$ is the $(N \times M)$ global ablation boundary coefficient matrix (the assembly of the $[B]^{(e)}$ matrices) and $\dot{s}^{n+1}$ is the vector of $M$ nodal recession rates along the ablating surface.

As with Eq. (18), there are $N$ unknown nodal temperatures, $M$ unknown nodal recession rates, and $N$ discrete conservation of energy equations. However, for the nodes along the ablating surface, each node will either be ablating or not ablating. For the nodes that are ablating, the nodal temperature is fixed at the ablation temperature and the recession rate is computed using the discrete conservation of energy equation for that node as represented in Eq. (19). For those nodes that are not ablating, the nodal recession rate is zero and the nodal temperature is computed using the discrete conservation of energy equation for that node. Because one of these conditions will exist for each of the $M$ potentially ablating nodes, the global system of equations [Eq. (19)], represents $N$ equations with only $N$ unknowns (temperatures and recession rates). During each time step, this equation is solved to obtain a vector of temperatures and recession rates satisfying conservation of energy.

To advance the solution a time step, begin with $T^n$ and $\dot{s}^n$ from the previous time step as initial guesses and iterate using an iteration index, i. Set $\dot{s}^i = \dot{s}^n$ and $T^i = T^n$.

1. Move the mesh based on $\dot{s}^i$
2. Build global system of equations with ablation boundary terms explicitly represented (Eq. (19))
3. Using $\dot{s}^i$, solve for the temperature vector from $[K]\,T^{i+1} = r - [B]\,\dot{s}^i$
4. For ablating nodes, if $T > T_f$ set $T = T_f$ and denote the modified temperature vector as $T^*$
5. Using $T^*$, solve the surface energy balance equations for the recession rate using $[B]\,\dot{s}^{i+1} = r - [K]\,T^*\big|^{i+1}$
6. Compute an average change of recession rate for ablating nodes between the $i+1$ and $i$ iteration using $\varepsilon = \frac{1}{M}\sum_{j=1}^{M}\left|\dot{s}_j^{\,i+1} - \dot{s}_j^{\,i}\right|$,
7. If $\varepsilon \geq \varepsilon_{max}$, then, using $\dot{s}^{i+1}$, return to Step 1

**Fig. 3 Flow chart showing the iterative procedure for solving conservation of energy with $Q^*$ ablation boundary conditions.**

The symbolic nature of Eq. (19) hides some of the details necessary to understand and implement this approach. The temperature coefficient matrix $K$ is a $(N \times N)$ matrix, whereas the recession rate matrix $B$ is a sparsely filled $(N \times M)$ matrix with nonzero contributions in only $M$ rows. Only ablating boundary nodes will have nonzero contributions in the $B$ matrix. Consequently, although the $B$ matrix is represented as a $(N \times M)$ matrix, it actually has contributions to the control volumes (equations) for only the $M$ nodes on the ablating boundary. In our implementation, we have exploited the nodal connectivity along the ablating boundary (for element types with two-node linear variations along the exposed sides) and stored the $B$ matrix as a tridiagonal matrix.

Figure 3 shows a flow chart that describes the iteration procedure for computing the unknown temperatures and recession rates to advance the solution over a time step with the boundary conditions described using the heat of ablation $Q^*$ approach. Again, it is assumed at the beginning of this iterative process that initial guesses of the temperature and recession rate are available from the previous solution. For the first time step, the recession rates are assumed to be zero.

#### Thermal-Grid Motion Coupling Algorithm

The equations describing the coupled heat conduction and grid motion can be solved using either a segregated or a fully coupled solution algorithm, depending on how tightly the two systems of equations are coupled in the problem. In the work presented here, a segregated solution algorithm is utilized; at convergence, both approaches yield identical results. In this approach, a Picard iteration is used at each time step to sequentially compute the temperature distribution and grid motion. Upon convergence, the computed temperatures and displacements satisfy the system of equations at time $n+1$. This sequential solution approach has proven to be adequate for the transient heat conduction and ablation problems we have considered. For other problems, such as steady-state solutions, where the grid motion and field equations are more tightly coupled, a fully coupled solution algorithm may be necessary. This approach is presently being investigated for other applications such as free surface flows and coating flows.[14]

## Computed Results

To evaluate the accuracy and demonstrate the applicability of this approach, two example problems are presented. For all calculations presented here, a fully implicit time integration scheme with first-order accuracy was used and the linear algebraic equations were solved using the direct band solver method of Gopalakrishnan and Palaniappan.[15] All calculations reported here were performed on a Sun SPARCstation 10™ using double precision.

#### One-Dimensional Problem with Analytical Solution

One-dimensional problems provide some of the few analytical solutions for ablation problems that can be used to benchmark computer programs. Consequently, to check the implementation of the ablation boundary conditions, to evaluate the accuracy of this approach, and to demonstrate the convergence characteristics of this approach, predicted results are compared with an exact solution for a one-dimensional ablation problem proposed by Storti.[16] In this problem, an analytical solution to a nonablating conduction problem is used to provide the analytical solution to an ablation problem by tracking the motion of a hypothetical phase change isotherm. The boundary condition of this example corresponds to $Q^*$ boundary condition.

The equation describing one-dimensional heat conduction within a semi-infinite solid is given by

$$\rho c_p \frac{\partial T}{\partial t} - \frac{\partial}{\partial x}\left(k\frac{\partial T}{\partial x}\right) = 0 \tag{20}$$

with boundary conditions given as

$$T(0, t) = T_w \quad \text{and} \quad T(\infty, t) = T_0 \tag{21}$$

and initial conditions as

$$T(x, 0) = T_0 \tag{22}$$

The analytical solution to Eq. (20), subject to the previous conditions, is available in most heat conduction books as

$$\frac{T(x, t) - T_w}{T_0 - T_w} = \operatorname{erf}\left(\frac{x}{2\sqrt{\alpha t}}\right) \tag{23}$$

To simulate an ablation boundary condition for a material ablating at $T_f$, where $T_0 < T_f < T_w$, the boundary condition at the location of the $T = T_f$ isotherm is tracked as the thermal wave penetrates the solid. The transient heat conduction problem is transformed into an ablation problem by applying a transient heat flux, computed analytically by differentiating Eq. (23), at the location of the $T = T_f$ isotherm. For time greater than zero, the heat flux occurring at the location of the $T = T_f$ isotherm and applied to the hypothetical ablating surface is given by

$$\dot{q}''(x) = \frac{k(T_w - T_0)}{\sqrt{\pi\alpha t}} \exp\left(-\frac{x^2}{4\alpha t}\right) \tag{24}$$

Because the heat flux is infinite at time zero, the numerical simulation begins after some finite time has elapsed, $t_0$. The location of the moving surface $x = s(t)$, which follows the

$T[s(t), t] = T_f$ isotherm can be determined from Eq. (23) and is

$$\frac{s(t)}{2\sqrt{\alpha t}} = \text{erf}^{-1}\left(\frac{T_w - T_f}{T_w - T_0}\right) \tag{25}$$

To simulate the ablation problem for $t > t_0$, the $T = T_f$ isotherm is tracked and the transient heat flux given by Eq. (24) is applied to the hypothetical ablating surface. The corresponding analytical expression for the surface recession rate can be obtained by differentiating Eq. (25) with respect to time, which results in

$$\dot{s}(t) = \sqrt{\frac{\alpha}{t}}\,\text{erf}^{-1}\left(\frac{T_w - T_f}{T_w - T_0}\right) \tag{26}$$

Note that $\dot{s}(t) \sim 1/\sqrt{t}$. In the example problem considered here, the simulated ablation problem was arbitrarily chosen to begin at $t_0 = 1$ s.

The ablation problem was solved using the following parameters: $T_0 = 300$ K, $T_w = 1300$ K, $T_f = 800$ K, and $\alpha_w = 1.0$ (absorptance). The thermal properties of the ablating material were assumed to be constant and are $\rho = 2$ g/cm$^3$, $C_p = 1$ J/g-K, $k = 0.002$ W/cm-K, and $Q^* = 2000$ J/g. The domain considered in this example extended from $0 \leq x \leq L$, where $L = 0.5$ cm.

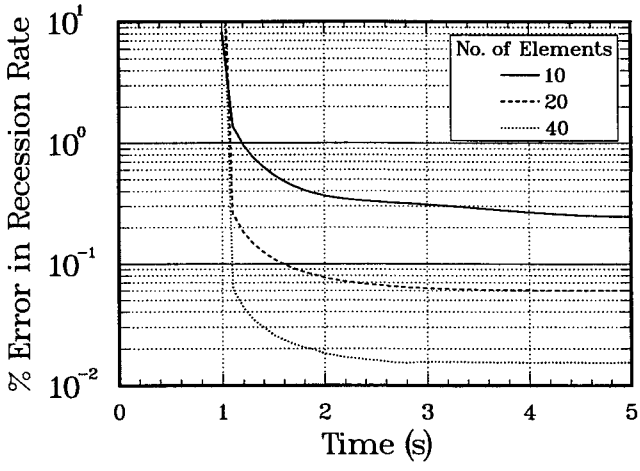


**Fig. 4 Percent error in recession rate as a function of time as the number of elements is increased.**

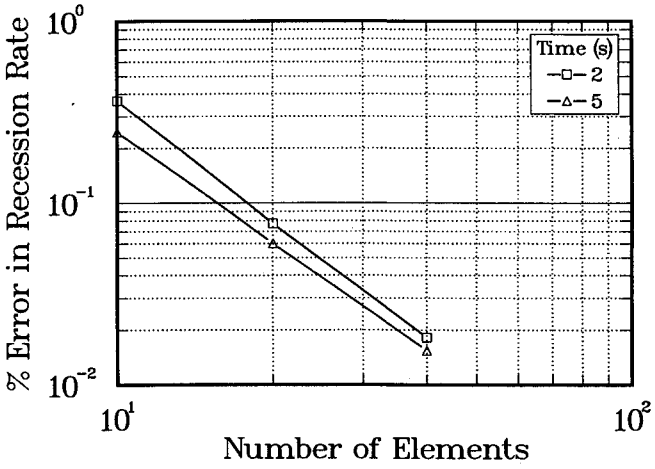


**Fig. 5 Percent error in recession rate decreases with increasing grid refinement. Approximate quadratic convergence is demonstrated with the CVFEM for two selected times.**

For the purposes of comparing the predicted recession rate with the analytical solution, a percent error in the recession rate is computed from

$$\varepsilon_s = 100 \times \left[\frac{\dot{s}(t)|_{\text{computed}}}{\dot{s}(t)|_{\text{analytical}}} - 1.0\right] \tag{27}$$

Figure 4 shows the percent error in recession rate as a function of time for varying numbers of elements in the solid. Clearly, as the number of elements increases, the solution is better resolved, and the percent error decreases. The error also decreases with time.

Figure 5 demonstrates that the percent error in the recession rate decreases approximately quadratically with the CVFEM as the number of elements is increased. This mesh refinement study was performed while keeping $\alpha\Delta t/\Delta x_1^2$ fixed, and the observed convergence behavior has also been observed in our previous work.[5]

### Axisymmetric Re-Entry Vehicle

To demonstrate the practical applicability of this approach, an analysis of a nose tip subjected to aerodynamic heating is presented. Figure 6 shows the initial grid used for the analysis of this vehicle. The body is divided into an outer region in which the grid is moving with time and an inner region in which the grid is fixed in space. In this approach, conservation of energy is solved over both regions with the solid mechanics equations solved only over the moving grid region. The interface between the fixed and moving grid regions must be chosen so that the final ablated shape does not cross this boundary.

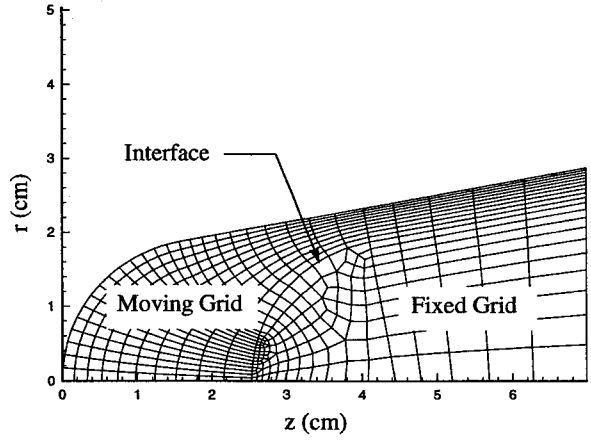


**Fig. 6 Schematic of initial grid showing the initial mesh and the interface between the moving and stationary regions for the axisymmetric nose tip.**

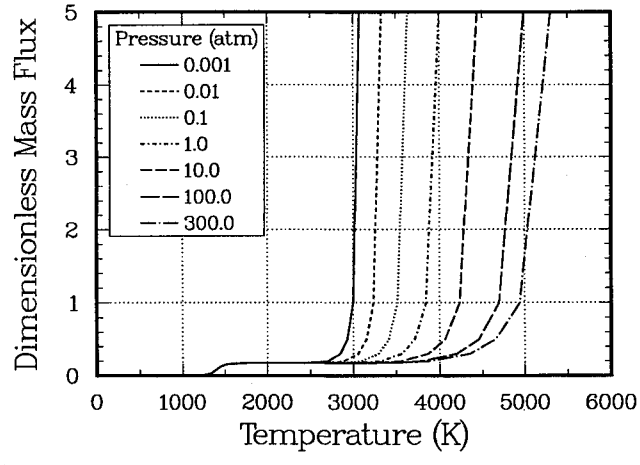


**Fig. 7 Dimensionless mass loss flux for graphite as a function of temperature and pressure.**

**Table 1 Cumulative number of elements within ranges of element angle standard deviations**

| | 0–3 | 0–6 | 0–9 | 0–12 | 0–15 | 0–18 | 0–21 |
|---|---|---|---|---|---|---|---|
| Spines | 96 | 172 | 244 | 275 | 298 | 300 | 300 |
| Solid mechanics | 116 | 201 | 261 | 289 | 297 | 299 | 300 |

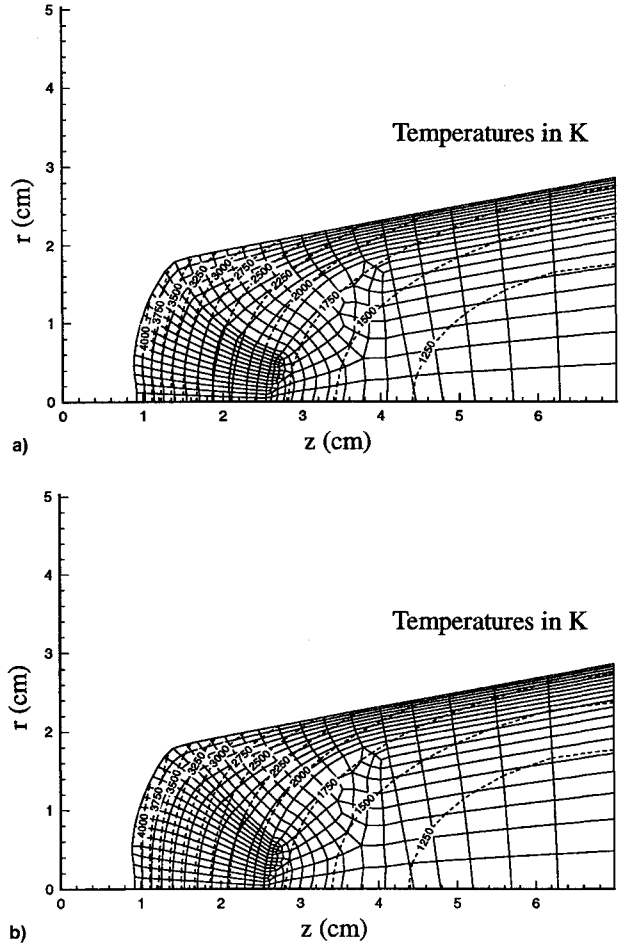


**Fig. 8 Predicted temperature distribution and body shape for 21.0 s computed by moving the grid using a) the spines approach and b) the linear elastic solid mechanics approach.**

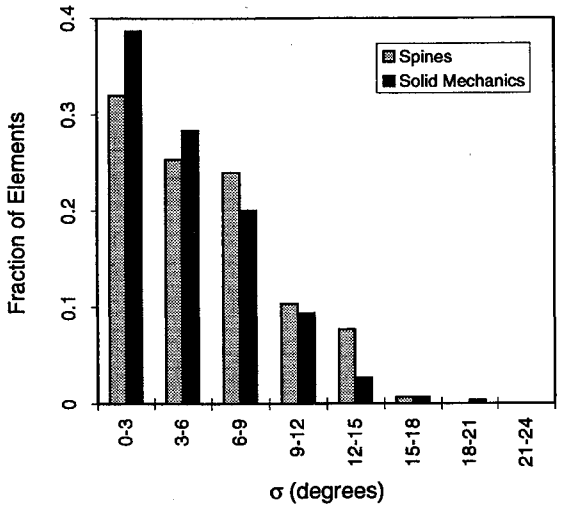


**Fig. 9 Distribution of variance in deviation of element angles from 90 deg demonstrating that the mesh moved using the solid mechanics approach is more orthogonal than the mesh moved using the spines approach.**

The ablator for this problem is graphite with representative temperature-dependent material properties. The ablation process for graphite is assumed to be described with the generalized thermochemical formulation [Eq. (7)]. Figure 7 shows the variation of dimensionless mass flux as a function of temperature for a range of pressures. In the code, this nonlinear dependence of mass flux on temperature and pressure is accounted for during the solution process. The initial temperature of the nose tip is 298 K.

The aerodynamic heating boundary conditions were computed using the HIBLARG computer code,[17] which solves the integral form of the momentum and energy equations along inviscid streamlines in a hypersonic boundary layer. The code predicts the aerodynamic heating boundary conditions used in the thermal code. In this example, the aerodynamic heating was computed for the initial geometry and applied to the nose tip over the duration of the flight. Consequently, the change in heat transfer to the body as the shape of the nose tip changes is not explicitly represented in the aerodynamic boundary conditions. The coupling between the boundary conditions and the shape change was done only in an approximate manner. To better simulate this problem, the aerodynamic heating code should be more tightly coupled with the ablation code and the evolving body shape. We are presently considering a procedure to improve this aspect of the simulation.

Figure 8 shows the computed temperature contours and body shape computed using the spines approach and the linear elastic solid mechanics approach. With both approaches, the isotherms are nearly identical. In general, the grid computed with the solid mechanics approach appears to be a better quality grid than the grid computed with the spines approach. The elements appear to have less skewness (to be more orthogonal) and are more orthogonal to the ablating surface. It is also interesting that the grid lines are concave downward for the solid mechanics approach and concave upward for the spines approach, even though both started from the same initial grid (Fig. 6). The two approaches differ in that the spines approach forces nodes to move along the original grid lines while the solid mechanics approach allows the interior nodes to move in any direction.

A quantitative assessment of the mesh quality is provided by computing the variance of the difference between interior angles and 90 deg for each element. This measure represents the deviation of the element from an orthogonal element. For example, an orthogonal element will have a variance of zero. An expression for this measure is given by

$$\sigma^2 = \frac{1}{4}\sum_{i=1}^{4}(\alpha_i - 90)^2 \tag{28}$$

where $\alpha_i$ is the interior angle (in degrees) for the element. Figure 9 shows the fraction of elements vs standard deviation in the difference between the interior angles of the elements and 90 deg for the meshes shown in Fig. 8. The data in Fig. 9 are divided into intervals of 3 deg. The mesh obtained with the solid mechanics approach has a greater fraction of elements within the 0–3 and 3–6 intervals and fewer elements in the intervals with $\sigma > 6$. Consequently, the mesh that evolved from the solid mechanics approach is of better quality (as defined previously) than the mesh computed using the spines approach.

Table 1 presents the cumulative number of elements as a function of standard deviation of element angle ranges as the range is increased. These results demonstrate that the solid mechanics approach has more elements than the spines approach up to the 0–15 range. For the 0–15 range and above, the two methods have essentially the same number of elements.

These results present a comparison of two approaches for computing grid motion. The linear elastic approach produces better quality grids, has greater generality, and can be applied to fully unstructured grids. Additionally, the extension to three-dimensional problems is straightforward. However, it requires more memory as well as more computational time (approximately 2.5 times as long for this two-dimensional example). Techniques to reduce the time requirements for the solid mechanics approach are presently being investigated.

## Concluding Remarks

An approach for solving two-dimensional axisymmetric ablation problems with unstructured grids has been presented. This approach uses a solid mechanics formulation with an unstructured mesh to compute the shape of the ablating body. One advantage of this procedure is that it removes all of the structured grid requirements of most other methods and is easily extended to three-dimensional problems. It also provides the framework for moving an unstructured grid with a small probability of mesh entanglement.

Example problems demonstrated the accuracy and convergence of this approach as well as the applicability to realistic problems. In general, the solid mechanics approach resulted in better quality meshes than the spines approach. Boundary conditions have been formulated and implemented for both heat of ablation and generalized thermochemical ablation boundary conditions.

## Acknowledgments

This work was performed at Sandia National Laboratories and was supported by the U.S. Department of Energy under Contract DE-AC04-94AL85000.

## References

[1]Brogan, J. J., "A Numerical Method of Solution for Heat Conduction in Composite Slabs with a Receding Surface," Lockheed Missiles and Space Division, Lockheed Aircraft Corp., LMSD 288204, Sunnyvale, CA, Jan. 1960.

[2]Moyer, C. B., and Rindal, R. A., "An Analysis of the Coupled Chemically Reacting Boundary Layer and Charring Ablator, Part II, Finite Difference Solution for the In-Depth Response of Charring Materials Considering Surface Chemical and Energy Balances," NASA CR-1061, June 1968.

[3]Landau, H. G., "Heat Conduction in a Melting Solid," *Quarterly of Applied Math*, Vol. VIII, No. 1, 1950, pp. 81–94.

[4]Blackwell, B. F., and Hogan, R. E., "One-Dimensional Ablation Using Landau Transformation and Finite Control Volume Procedure," *Journal of Thermophysics and Heat Transfer*, Vol. 8, No. 2, 1994, pp. 282–287.

[5]Blackwell, B. F., and Hogan, R. E., "Numerical Solution of Heat Conduction Problems Using a Finite Control Volume Technique," *Journal of Thermophysics and Heat Transfer*, Vol. 7, No. 3, 1993, pp. 462–471.

[6]Blackwell, B. F., Thornton, A. L., and Hogan, R. E., "Ablation Problems Using a Finite Control Volume Technique," *Proceedings of the Moving Boundary 93 Conference* (Milan, Italy), 1993, pp. 295–302.

[7]Hogge, M., and Gerrekens, P., "One-Dimensional Finite Element Analysis of Thermal Ablation with Pyrolysis," *Computer Methods in Applied Mechanics and Engineering*, Vol. 33, Nos. 1–3, 1982, pp. 609–634.

[8]Hogge, M., and Gerrekens, P., "Two-Dimensional Deforming Finite Element Methods for Surface Ablation," *AIAA Journal*, Vol. 23, No. 3, 1985, pp. 465–472.

[9]Lynch, D. R., and Gray, W. G., "Finite Element Simulation of Flow in Deforming Regions," *Journal of Computational Physics*, Vol. 36, No. 2, 1980, pp. 135–153.

[10]Lynch, D. R., and O'Neill, K., "Continuously Deforming Finite Elements for the Solution of Parabolic Problems, With and Without Phase Change," *International Journal for Numerical Methods in Engineering*, Vol. 17, No. 1, 1981, pp. 81–96.

[11]King, H. H. C., Muramoto, K. K., Murray, A. L., and Pronchick, S. W., "ABRES Shape Change Code (ASCC 86)," Acurex Corp., BMO TR-87-57, Mountain View, CA, Dec. 1986.

[12]Reddy, J. N., *An Introduction to the Finite Element Method*, McGraw–Hill, New York, 1984.

[13]Lynch, D. R., and O'Neill, K., "Elastic Grid Deformation for Moving Boundary Problems in Two Space Dimensions," *Finite Elements in Water Resources III*, Vol. 2, edited by Wang et al., Mississippi Univ., Oxford, MS, 1980, pp. 7.111–7.120.

[14]Schunk, P. R., Sackinger, P. A., Hogan, R. E., and Blackwell, B. F., 7th International Coating Process Science and Technology Symposium, AIChE 1994 Spring National Meeting, Atlanta, GA, 1994.

[15]Gopapaiakrishnan, T. C., and Palaniappan, A. B., "Band Algorithm for Unsymmetric Matrices in Finite Element and Semi-Discrete Methods," *International Journal for Numerical Methods in Engineering*, Vol. 18, No. 8, 1982, pp. 1197–1211.

[16]Storti, M., "Numerical Modeling of Ablation Phenomena as Two-Phase Stefan Problems," *International Journal of Heat and Mass Transfer*, Vol. 38, No. 15, 1995, pp. 2843–2854.

[17]Polansky, G. F., "Hypersonic Integral Boundary Layer Analysis of Reentry Geometries (HIBLARG) Code Description and User's Manual Version 2.0," Sandia National Labs., SAND89-0552, Albuquerque, NM, March 1990.